

# Functional renormalization group study of neutral and charged pion under magnetic fields in the quark-meson model

Rui Wen,<sup>1,\*</sup> Shi Yin,<sup>2</sup> Wei-jie Fu,<sup>2</sup> and Mei Huang<sup>1,†</sup>

<sup>1</sup>*School of Nuclear Science and Technology, University of Chinese Academy of Sciences, Beijing, 100049, P.R. China*

<sup>2</sup>*School of Physics, Dalian University of Technology, Dalian, 116024, P.R. China*

We calculated the masses of neutral and charged pion and pion decay constants under an extra magnetic field at zero temperature. The quantum fluctuations are integrated through the functional renormalization group. We consider the quark and meson propagators in the Landau level representation and weak-field expansion, respectively. The neutral pion mass monotonically decreases with the magnetic field, while the charged pion mass monotonically increases with the magnetic field. The pion decay constant and the quark mass show the magnetic catalysis behavior at vanishing temperature. The neutral pion mass and pion decay constant are quantitatively in agreement with the lattice QCD results in the region of  $eB < 1.2\text{GeV}^2$ , and no non-monotonic mass behavior for charged pion has been observed in this framework.

## I. INTRODUCTION

Studying Quantum Chromodynamics (QCD) matter under strong external magnetic field and vortical field have attracted many attentions in recent years. Relativistic heavy-ion collisions provide us a platform to study QCD matter under extreme conditions in the laboratory. In non-central heavy-ion collisions, the collision of two high-speed nuclei moving in opposite directions could create strong magnetic fields of order  $\sim 10^{18}$  Gauss [1, 2]. Strong magnetic fields also exist in the early universe and magnetars [3–5]. Understanding the strongly interacting matter in background magnetic fields requires a combination of the QCD and QED theories, which has brought about plenty of novel phenomena of magnetized quark matter, such as the chiral magnetic effect (CME) [6, 7], magnetic catalysis (MC) [8–10], inverse magnetic catalysis (IMC) [11–13], diamagnetism at low temperature and paramagnetism at high temperature [14]. These rich phenomena have attracted theoretical investigations in lattice Monte-Carlo simulations [15–21], as well as model calculations, such as Nambu-Jona-Lasinio (NJL) [22–28], quark-meson (QM) model [29–31] and AdS/QCD [32, 33], within mean-field approximation or functional methods [34–38], see e.g., [39–42] for reviews.

It is also valuable to study the meson spectrum of QCD under magnetic fields, which plays an important role in the understanding of the rich phenomena mentioned above. It is believed that the neutral pion is helpful to explain the inverse magnetic catalysis [43, 44], and the charged pions can explain the diamagnetic around the pseudo-critical temperature [38]. The meson spectra have been widely studied in lattice QCD and effective models [16–18, 45–51]. Recent Lattice calculation in [20] showed that at zero temperature, the mass of the neutral  $\pi$  meson decreases monotonously with the magnetic field, while that of the charged pions shows a non-monotonic

behavior. Some efforts have been made to understand the pion mass behavior under magnetic field in low energy effective models [52–56]. However, the mass behaviors of the neutral and charged pions under magnetic field have not been explained simultaneously. Besides, the lattice and effective model calculations are also extended to finite temperatures, see e.g., [21, 57–60].

In this work, we employ the quark-meson model, which is also called the linear sigma model coupled to quarks (LSMq) [29, 61] to calculate the meson masses and decay constants under a magnetic field. This model is well used to study the QCD phase diagrams [62, 63], Equation of State (EoS) [64, 65] as well as the fluctuations of conserved charges [66, 67]. Note that it can be transformed from the NJL model through a Hubbard-Stratonovich transformation [68, 69]. The results of the mean-field approximation of the QM model coincide with the point-like particles. In this work, we include the quantum fluctuations through the functional renormalization group approach (FRG) [70, 71], which is a functional continuum field approach.

This paper is organized as follows. In [Section II](#), we introduce the low energy effective theory, i.e. the 2-flavor quark meson model. In [Section III](#), the choice of the regulator, propagators under a magnetic field are discussed and the flow equations are presented. In [Section IV](#), we show the numerical results in our calculation, including the meson masses, quark masses and decay constants as functions of the strength of magnetic field. In [Appendix A](#), we show the vertexes of the 2-flavor quark meson model. In [Appendix B](#), the threshold functions of the flow equations are given.

## II. LOW ENERGY EFFECTIVE THEORY

At high renormalization group (RG) scale, the first-principle QCD system only includes the degrees of freedom of quarks and gluons. As the RG scale decreases, due to the finite mass gap, the gluons are decoupled from the system, and their dynamics are integrated out, left

\* [rwen@ucas.ac.cn](mailto:rwen@ucas.ac.cn)

† [huangmei@ucas.edu.cn](mailto:huangmei@ucas.edu.cn)

with gluonic background field and its potential. Consequently, composite degrees of freedom, e.g., mesons and baryons, emerge naturally from the dynamics of elementary degrees of freedom, see, e.g., [72–74]. The degrees of freedom of the QCD system are transformed into those of quarks and hadrons, which can be described by low-energy effective models, such as the QM model and NJL model.

The effective action of the two-flavor quark-meson model in Euclidean space reads [75]

$$\Gamma_k = \int_x \bar{q} \gamma_\mu (\partial_\mu - iQ A_\mu) q + \text{Tr}(D_\mu \phi \cdot D_\mu \phi^\dagger) + h\bar{q}(T^0 \sigma + i\gamma_5 \vec{T} \cdot \vec{\pi})q + V_k(\rho) - c\sigma, \quad (1)$$

with  $\int_x = \int d^4x$ ,  $Q = \text{diag}(2/3, -1/3)e$  and  $q = (u, d)^T$ . Here,  $\phi$  denotes the meson fields:

$$\phi = T^0 \sigma + \vec{T} \cdot \vec{\pi} = \frac{1}{2} \begin{pmatrix} \sigma + \pi^0 & \sqrt{2}\pi^+ \\ \sqrt{2}\pi^- & \sigma - \pi^0 \end{pmatrix}. \quad (2)$$

In Equation (1), the potential  $V(\rho)$  is chiral symmetric with  $\rho \equiv \text{Tr}[\phi^\dagger \phi] = \frac{1}{2}(\sigma^2 + \vec{\pi}^2)$ , and  $c\sigma$  is the linear sigma term, which explicitly breaks the chiral symmetry and accounts for the pion masses. The covariant derivative of meson fields reads

$$D_\mu \phi = \partial_\mu - iA_\mu[Q, \phi]. \quad (3)$$

Without loss of generality, a homogeneous magnetic field of strength  $B$  is assumed along the  $z$ -direction and the Landau gauge is adopted, i.e.  $A_\mu = (0, 0, xB, 0)$ . For convenience, we define  $p_\perp = (p_1, p_2)$  and  $p_\parallel = (p_0, p_3)$ .

The curvature masses are defined as the two-point correlation function at vanishing external momentum

$$m_{\phi, \text{cur}}^2 = \Gamma_{\phi\phi}^{(2)}(p_0 = 0, \vec{p} = 0), \quad (4)$$

and for the  $\pi$  and  $\sigma$  meson, they are given as

$$m_\pi^2 = V'(\rho) \quad m_\sigma^2 = V'(\rho) + 2\rho V''(\rho). \quad (5)$$

The light quark mass is

$$m_q = \frac{1}{2} h \sigma_0. \quad (6)$$

Here  $\sigma_0$  is the vacuum expectation value of the sigma meson field, which is located at the minimum of the effective potential. The mesonic decay constant is also related to the vacuum expectation value via:

$$f_\pi = \sigma_0. \quad (7)$$

In this work, we employ the local potential approximation (LPA), which is the leading order of the derivative expansion. In other words, we ignore the mesonic and quark wave function renormalizations and the running of the Yukawa coupling. See [30] for a relevant discussion, where magnetic dependent wave function renormalizations beyond LPA are investigated in one-flavor case within the FRG approach.

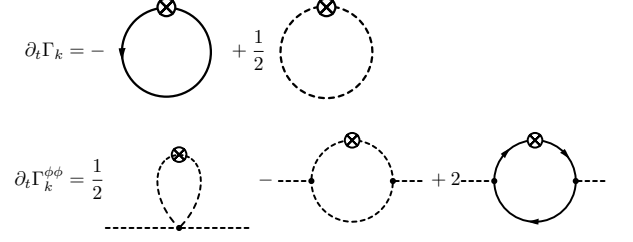


FIG. 1: Feynman diagrams of the flow equations for the effective potential (upper) and the mesonic two-point correlation functions (lower). The solid lines and dashed lines denote the quark and meson propagators, respectively. The crossed circles denotes the infrared regulators, as shown in Equation (9).

### III. FLOW EQUATIONS AND REGULATORS

The evolution of the effective action with the RG scale is described by the Wetterich equation [76], where an infrared (IR) cutoff scale  $k$ , i.e., the RG scale, is used to suppress quantum fluctuations of momenta below the scale. Starting from a high ultraviolet (UV) scale, say  $\Lambda_{\text{UV}}$ , with the classical action as the initial condition, one is able to integrate-in quantum fluctuations of different modes successively by evolving the RG scale  $k$  from UV to IR. The Wetterich equation for the effective action Equation (1) reads:

$$\partial_t \Gamma_k = \frac{1}{2} \text{Tr}[G_k^\phi(p) \partial_t R_k^B] - \text{Tr}[G_k^q(p) \partial_t R_k^F]. \quad (8)$$

Here  $R_k$  denotes the regulators and  $G_k^{\phi/q}(p)$  are scale-dependent propagators of mesons and quarks.

In the vacuum, the effective action satisfies the  $O(4)$  space-time symmetry. When we consider an external magnetic field, the perpendicular (transverse) and parallel (longitudinal) directions to the magnetic field will split. Obviously, it will stay invariant in the temporal and  $z$  directions at zero temperature. A commonly used  $3d$  regulator for the spatial momenta breaks the  $O(4)$  symmetry in the vacuum [77], while a regularization on the transverse momenta would give rise to non-physical artifacts [78]. Therefore, in this work we adopt  $2d$  regulators which regularize the temporal and longitudinal momenta, as follows

$$R_k^B = p_\parallel^2 r_B(p_\parallel^2/k^2), \\ R_k^F = i p_\parallel \cdot \gamma_\parallel r_F(p_\parallel^2/k^2), \quad (9)$$

with  $p_\parallel^2 = p_0^2 + p_3^2$  and the shape functions

$$r_B(x) = \left(\frac{1}{x} - 1\right) \Theta(1-x) \\ r_F(x) = \left(\frac{1}{\sqrt{x}} - 1\right) \Theta(1-x). \quad (10)$$

Here  $\Theta(x)$  is the Heaviside step function. Notably, absence of regularization on the transverse momenta leads to a divergence for the flow equation of the potential  $V_k$ . Fortunately, the two-point correlation functions stay finite [30]. The summation of the Landau level can be calculated through the Hurwitz  $\zeta$ -function [40]

$$\zeta(s, q) = \sum_n \frac{1}{(q+n)^s}. \quad (11)$$

In this work, we use a transverse momentum cutoff  $\Lambda_\perp = 5\text{GeV}$  to calculate the  $u$ - $d$  quark mixed threshold functions. We have checked that our results show no obvious dependence on the choices.

### A. propagators and flow equations

The quark propagator in magnetic fields in the Schwinger scheme reads

$$G(x, y) = e^{i\Phi(x_\perp, y_\perp)} \int \frac{d^4 p}{(2\pi)^4} e^{-ip(x-y)} \tilde{G}(p). \quad (12)$$

Where prefactor  $\Phi(x_\perp, y_\perp) = s_\perp(x^1 + y^1)(x^2 - y^2)|q_f B|/2$  with  $s_\perp \equiv \text{sign}(q_f B)$  is the Schwinger phase [79], which breaks the translational invariance. In this work, we ignore the Schwinger phase of the propagators under magnetic fields, and see, e.g., [25, 80] for more discussions on the Schwinger phase with the Ritus scheme. Recently, it has been found that the Schwinger phase can be neglected when the meson masses are calculated [50]. The translationally invariant part of the quark propagator in the representation of Landau levels in the Euclidean space with the regulator reads [30, 40]:

$$\tilde{G}_k^q(p) = \exp\left(-\frac{p_\perp^2}{|q_f B|}\right) \sum_{n=0}^{\infty} \frac{(-1)^n D_n(p_\parallel, R_F, p_\perp)}{p_\parallel^2, R_F + 2n|q_f B| + m_f^2}, \quad (13)$$

with  $p_\parallel, R_F \equiv p_\parallel(1 + r_F)$  and

$$\begin{aligned} & D_n(p_\parallel, p_\perp) \\ &= (-i\gamma_\parallel p_\parallel + m_f) \left[ (1 + i\gamma_1 \gamma_2 s_\perp) \mathcal{L}_n\left(\frac{2p_\perp^2}{|q_f B|}\right) \right. \\ & \quad \left. - (1 - i\gamma_1 \gamma_2 s_\perp) \mathcal{L}_{n-1}\left(\frac{2p_\perp^2}{|q_f B|}\right) \right] \\ & \quad + 4i\gamma_\perp p_\perp \mathcal{L}_{n-1}^1\left(\frac{2p_\perp^2}{|q_f B|}\right). \end{aligned} \quad (14)$$

Here  $\mathcal{L}_n^a(x)$  are the generalized Laguerre polynomials with  $\mathcal{L}_{-1}^a(x) = 0$ . Similarly, the translationally invariant part of the scale-dependent meson propagator reads

$$\begin{aligned} \tilde{G}_k^\phi(p) &= 2 \exp\left(-\frac{p_\perp^2}{|q_\phi B|}\right) \\ & \times \sum_{n=0}^{\infty} \frac{(-1)^n \mathcal{L}_n\left(\frac{2p_\perp^2}{|q_\phi B|}\right)}{p_\parallel^2, R_B + (2n+1)|q_\phi B| + m_\phi^2}. \end{aligned} \quad (15)$$

with  $p_\parallel, R_B \equiv p_\parallel(1 + r_B)^{\frac{1}{2}}$ .

With the aforementioned setup, one is led to the flow equations of the effective potential:

$$\begin{aligned} \partial_t V_k &= \frac{1}{2} [l_B(m_\sigma) + l_B(m_{\pi^0}) + 2l_B(m_{\pi^\pm})] \\ & \quad - 4N_c [l_F(m_f, q_u) + l_F(m_f, q_d)]. \end{aligned} \quad (16)$$

The relevant Feynman diagrams are presented in the first line of **Figure 1**. Here  $l_B, l_F$  are threshold functions given in **Appendix B**. By taking the second derivative of **Equation (8)** with the pion fields, one arrives at the flow equation of two-point correlation function of the neutral pion as follows

$$\begin{aligned} \partial_t \Gamma_{\pi^0 \pi^0, k}^{(2)} &= \frac{1}{2} [V_{2\pi^0 2\sigma} \mathcal{J}_B(\sigma) + V_{4\pi^0} \mathcal{J}_B(\pi^0) \\ & \quad + 2V_{2\pi^0 2\pi^\pm} \mathcal{J}_B(\pi^\pm)] - V_{2\pi^0 \sigma}^2 \mathcal{J}_{2B}(\pi^0, \sigma) \\ & \quad + V_{uu\pi^0}^2 \mathcal{J}_F(u) + V_{dd\pi^0}^2 \mathcal{J}_F(d), \end{aligned} \quad (17)$$

and the flow equation of two-point correlation function of charged pions,

$$\begin{aligned} \partial_t \Gamma_{\pi^\pm \pi^\pm, k}^{(2)} &= \frac{1}{2} [V_{2\pi^\pm 2\sigma} \mathcal{J}_B(\sigma) + V_{2\pi^0 \pi^\pm} \mathcal{J}_B(\pi^0) \\ & \quad + 2V_{4\pi^\pm} \mathcal{J}_B(\pi^\pm)] - V_{2\pi^\pm \sigma}^2 \mathcal{J}_{2B}(\pi^\pm, \sigma) \\ & \quad + V_{ud\pi^\pm}^2 \mathcal{J}_{2F}(u, d). \end{aligned} \quad (18)$$

Here  $V_{[\dots]}$  denote different vertices listed in **Appendix A**, and  $\mathcal{J}_B, \mathcal{J}_{2B}, \mathcal{J}_F, \mathcal{J}_{2F}$  are threshold functions, which are defined in **Appendix B**. The corresponding Feynman diagrams are shown in the second line of **Figure 1**. It can be readily verified that the neutral pion flow equation **Equation (17)** coincides with the flow equation of first order derivative of the potential, i.e.,

$$\partial_t \Gamma_{\pi^0 \pi^0, k}^{(2)} = \partial_t V_k'(\rho). \quad (19)$$

### B. weak-field expansion

The number of Landau levels increases significantly in the region of small magnetic field. We do the computation in this region by utilizing the weak-field expansion method. The weak-field expansion for the quark propagator in the Euclidean space reads [81, 82]

$$\begin{aligned} \tilde{G}_k^q(p) &= \frac{-ip_{\mu, R_F} \gamma_\mu + m_f}{p_{R_F}^2 + m_f^2} + i \frac{\gamma_1 \gamma_2 (m_f - i\gamma_\parallel p_\parallel, R_F)}{(p_{R_F}^2 + m_f^2)^2} q_f B \\ & \quad + 2 \frac{p_\perp^2 (m_f - i\gamma_\parallel p_\parallel, R_F) + i\gamma_\perp p_\perp (m_f^2 + p_{\parallel, R_F}^2)}{(p_{R_F}^2 + m_f^2)^4} (q_f B)^2 \\ & \quad + \mathcal{O}(q_f B)^3. \end{aligned} \quad (20)$$

$\lambda_1 [\text{MeV}]^2$	$\lambda_2$	$h$	$c [\text{MeV}]^3$	$m_\pi [\text{MeV}]$	$m_\sigma [\text{MeV}]$	$m_q [\text{MeV}]$	$f_\pi [\text{MeV}]$
$(740)^2$	-5.0	6.4	$4.5 \times 10^6$	220	475	295	92
$(775)^2$	6.0	6.4	$1.6 \times 10^7$	416	675	295	92

TABLE I: Parameters for the initial conditions in [Equations \(1\) and \(25\)](#) and corresponding physical observables at  $B = 0$ . If not mentioned explicitly, most of the results are calculated with the parameters in the first line with  $m_\pi = 220$  MeV.

Thus, one arrives at the quark loop function for the two-point correlation function of charged pions, as follows

$$\begin{aligned} \mathcal{J}_{2F}(u, d) = & -\frac{k^4 N_c}{2\pi^2} \left[ \frac{\Lambda_\perp^2}{(k^2 + m_f^2)(k^2 + m_f^2 + \Lambda_\perp^2)} \right. \\ & + \left( \frac{1}{4(k^2 + m_f^2)^3} + \frac{5k^2 + 5m_f^2 + 8\Lambda_\perp^2}{12(k^2 + m_f^2 + \Lambda_\perp^2)^4} \right) (q_u B)(q_d B) \Big] \\ & + \mathcal{O}(B)^4. \end{aligned} \quad (21)$$

In the same way, the quark loops for the two-point correlation function of neutral pions read

$$\begin{aligned} \mathcal{J}_{2F}(q_f) = & -\frac{k^4 N_c}{2\pi^2} \left[ \frac{\Lambda_\perp^2}{(k^2 + m_f^2)(k^2 + m_f^2 + \Lambda_\perp^2)} \right. \\ & + \left( \frac{1}{4(k^2 + m_f^2)^3} + \frac{5k^2 + 5m_f^2 + 8\Lambda_\perp^2}{12(k^2 + m_f^2 + \Lambda_\perp^2)^4} \right) (q_f B)^2 \Big] \\ & + \mathcal{O}(B)^4. \end{aligned} \quad (22)$$

The weak-field expansion for the meson propagator reads [\[29, 83\]](#)

$$\begin{aligned} \tilde{G}_k^\phi(p) = & \frac{1}{p_{RB}^2 + m_\phi^2} + \frac{p_\perp^2 - p_{\parallel, RB}^2 - m_\phi^2}{(p_{RB}^2 + m_\phi^2)^4} (q_\phi B)^2 \\ & + \mathcal{O}(q_\phi B)^4. \end{aligned} \quad (23)$$

Then the weak-field expansions of the charged pion loop function  $\mathcal{J}_B(\pi^\pm)$  and the pion-sigma loop function  $\mathcal{J}_{2B}(\pi^\pm, \sigma)$  can be readily obtained, and their explicit expressions are listed in [Appendix B](#).

We find that the quark loops, as the last diagram in the second line of [Figure 1](#) shows, play the dominant role for the pion two-point correlation functions. When  $\Lambda_\perp \rightarrow \infty$ , the leading term in  $B$  reads  $1/(4(k^2 + m_f^2)^3) q_{f1} q_{f2} B^2$ . For the charged pion, the signs of  $q_u, q_d$  are opposite, so this term would make a negative contribution to the flow equation, implying that the contribution of quantum fluctuations to the charged pion mass is positive, which results in larger mass for charged pions in FRG than the point-like mass. On the contrary, for the neutral pion, the sign of  $q_u^2$  or  $q_d^2$  are positive. Consequently, the flow is increased and the mass of neutral pion is decreased in comparison to that in vacuum.

#### IV. NUMERICAL RESULTS

In this work, we solved the flow equation of effective potential by employing the Taylor expansion method

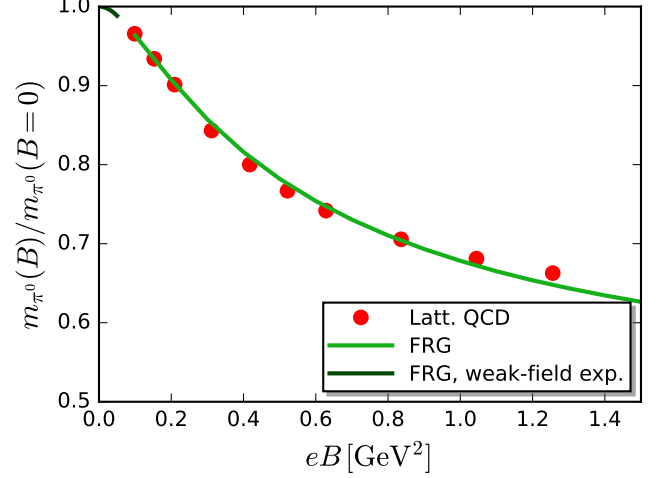


FIG. 2: Neutral pion mass  $m_{\pi^0}$  as a function of the strength of magnetic field. The lattice QCD results are taken from Ref [\[20\]](#).

around a fixed point, i.e.

$$V_k(\rho) = \sum_n^{N_v} \frac{\lambda_{n,k}}{n!} (\rho - \kappa)^n. \quad (24)$$

Here  $\kappa$  denotes the expanding point, located at the minimal value of the effective potential with  $k = 0$ . We choose the maximal order of the Taylor expansion to be  $N_v = 5$ , and for more discussions on the convergence of the Taylor expansion see [\[77, 84\]](#). We have also checked the physical-point expanding method, in which the expanding point is the minimal value of the effective potential at every value of the RG scale  $k$ . We find that these two methods coincide with each other and produce consistent results. The UV cutoff is chosen to be  $\Lambda_{UV} = 700$  MeV, where the initial condition of the effective potential reads

$$V_{UV}(\rho) = \lambda_1 \rho + \frac{\lambda_2}{2} \rho^2. \quad (25)$$

Here, the parameters of the initial conditions and the corresponding physical observables at  $B = 0$  are listed in [Table I](#). In order to compare with the lattice QCD results,  $m_\pi = 220$  MeV and  $m_\pi = 416$  MeV are chosen. Note that if not mentioned explicitly, most of the results are calculated with  $m_\pi = 220$  MeV.

In [Figure 2](#), we show the neutral pion mass  $m_{\pi^0}$  as a function of the strength of magnetic field in comparison to the Lattice QCD results [\[20\]](#). In the region of small magnetic fields with  $eB < 0.05[\text{GeV}^2]$ , we utilize the weak-field expansion method, while in other regions calculations are done through summation of the Landau levels. Our results are qualitatively or even quantitatively in agreement with the lattice results. If the neutral pion is regarded as a point particle, its masses will not change under magnetic fields. Due to the inner structure of the neutral pion, i.e.  $\bar{u}u$  or  $\bar{d}d$ , the neutral pion mass decreases with the magnetic field, as discussed in [Section III B](#). The neutral pion mass decreases monotonically with the increase of magnetic fields, and the rate of decrease is gradually reduced. Finally, it tends to saturate in large magnetic fields.

The charged pion mass  $m_{\pi^\pm}$  is defined as the lowest energy of quantum states for the charged pion [\[25\]](#), i.e.  $m_{\pi^\pm}(B) = E_{\pi^\pm}|_{p_z=0, n=0}$ . For the point particle of the charged pion, the mass is given by  $m_{\pi^\pm}(B) = \sqrt{m_{\pi^\pm}^2(B=0) + eB}$ . According to the definition, we need to calculate the two-point correlation function  $\Gamma_{\pi^\pm\pi^\pm}^{(2)}(p_\parallel = 0, p_\perp = |eB|)$ . Note, however, that it is challenging to integrate the loop functions  $\mathcal{J}_{2F}(u, d)$  and  $\mathcal{J}_{2B}(\pi^\pm, \sigma)$  with finite external momenta. In our calculation, we use the approximation as follows

$$m_{\pi^\pm}(B) = \sqrt{\Gamma_{\pi^\pm\pi^\pm}^{(2)}(p_\parallel = 0, p_\perp = 0) + eB}. \quad (26)$$

We also calculate  $\Gamma_{\pi^\pm\pi^\pm}^{(2)}(p_\parallel = 0, p_\perp = |eB|)$  at very large magnetic fields, and find that both results are consistent with each other.

In the left panel of [Figure 3](#), we plot the charged pion masses as functions of the strength of magnetic field with  $m_\pi(B=0) = 220$  MeV. In order to compare with the Lattice QCD results [\[20\]](#), where the computation is done with  $m_\pi(B=0) \sim 220$  MeV. We use lattice results of  $m_{\pi^\pm}^2(B) - m_\pi^2(B=0)$  and construct

$$m_{\pi^\pm}(B) = \sqrt{m_{\pi^\pm}^2(B) - m_\pi^2(B=0) + (220\text{MeV})^2}, \quad (27)$$

to be compared with FRG calculations. In the right panel of [Figure 3](#), we use the initial conditions in the second line in [Table I](#), corresponding to  $m_\pi(B=0) = 416$  MeV, and compare the normalized charged pion mass  $m_{\pi^\pm}(B)/m_\pi(0)$  with the lattice results with the same pion mass in the vacuum [\[17\]](#). The charged pion masses in our calculation increase monotonically with the magnetic field. Our results are larger than the point-like charged pion masses and in agreement with the lattice QCD results in [\[17\]](#). Similar results are also reported in the NJL calculation [\[25, 53\]](#). However, for the lattice calculations in [\[20\]](#), the charged pion masses are smaller than the point-like results and exhibit nonmonotonic behaviors. This means our results receive an opposite contribution from the quantum fluctuation compared to the

lattice QCD result in [\[20\]](#). The main contribution of quantum fluctuations comes from the  $u$ - $d$  quark loop, as discussed in the last paragraph of [Section III B](#), the leading order magnetic dependent quantum fluctuation of charged pion is opposite to that of the neutral pion, which could lead to the neutral pion masses smaller than point-like results and charged pion masses larger than point-like results in the region of weak magnetic field, as shown in the inlay in the left panel of [Figure 3](#). The calculation results with the Landau level representation coincide with those of weak-field expansion. On the one hand, this discrepancy between the charged pion mass obtained in our calculations and that in lattice simulations in [\[20\]](#) also probably arises from the approximations used in our calculations, such as neglect of the magnetic dependence of the Yukawa couplings and the wave function renormalizations. Our calculation is based on an effective model, which only contains the scalar and pseudoscalar channels, and other tensor structure channels and gluon dynamics are not taken into account [\[54\]](#). On the other hand, the opposite quantum contribution could come from the lattice QCD calculation. Notably, the lattice cutoff in [\[20\]](#)  $a \simeq 0.117$  fm and no continuum limit is done, while in [\[17\]](#) the continuum limit results are obtained, while the pion masses are much heavier than the physical value. Therefore, more detailed calculations and studies are required for both the lattice QCD and effective theories.

In [Figure 4](#), we plot the pion decay constant as a function of the strength of magnetic field and compared it with the lattice QCD results [\[20\]](#). For the 2-flavor QM model, the pion decay constant is determined by the minimum of the effective potential in [Equation \(7\)](#). In the QM model, one cannot distinguish the  $u$  or  $d$  pion decay constants, and our results are close to that of  $f_{\pi_d^0}$  in lattice QCD.

In [Figure 5](#), we show the magnetic dependence of the sigma meson mass and light quark mass. The lattice QCD results are constructed from the quark chiral condensates in Ref [\[20\]](#). Similar to the pion decay constant  $f_\pi$ , the light quark mass is close to the  $d$  quark results of the lattice QCD. Furthermore, due to the internal structure of mesons, the mass of sigma meson varies with the magnetic field. The sigma meson and light quark masses increase monotonically with the magnetic field. The decay constant, sigma meson mass, and light quark mass reflect chiral symmetry breaking increasing with magnetic fields, which is related to the magnetic catalysis.

## V. CONCLUSION

This work calculates the meson masses and the pion decay constant at vanishing temperature under strong magnetic fields. The quantum fluctuations are successfully included using the FRG approach. The two-point correlation functions of neutral and charged pion are calculated. The neutral pion mass monotonically decreases

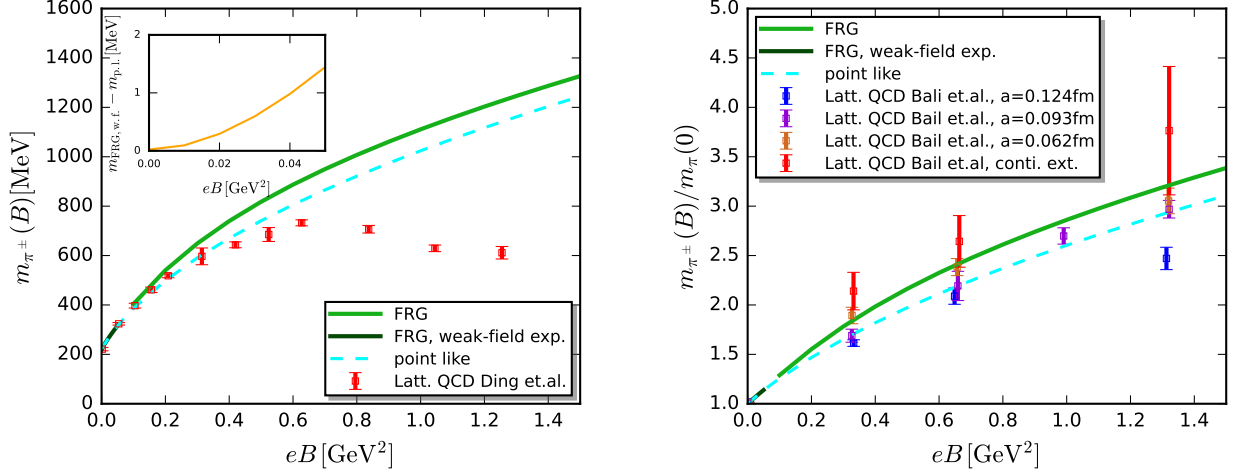


FIG. 3: Left panel: Charged pion mass  $m_{\pi^\pm}$  as a function of the strength of magnetic field with  $m_{\pi}(0) = 220$  MeV. The lattice QCD results are constructed based on data from Ref [20] and more details are shown in the text. In the inset, we show the charged pion mass in the weak-field expansion with FRG subtracted by the point-like result. Right panel: Normalized charged pion mass  $m_{\pi^\pm}(B)/m_{\pi}(0)$  as a function of magnetic fields with  $m_{\pi}(0) = 416$  MeV in comparison to the relevant Lattice QCD [17].

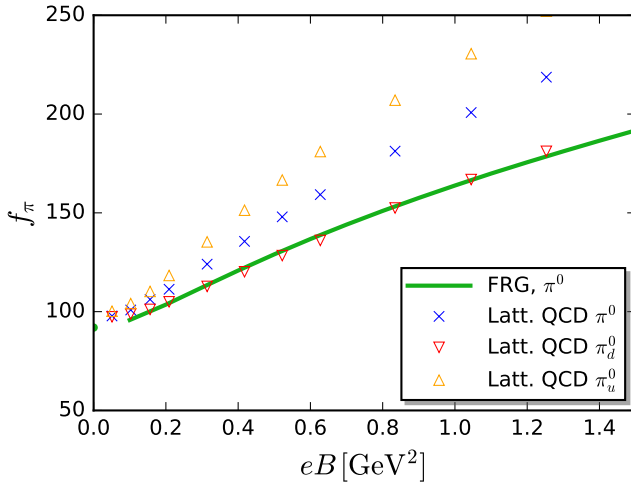


FIG. 4: Pion decay constant as a function of the strength of magnetic field. The lattice QCD results are taken from Ref [20].

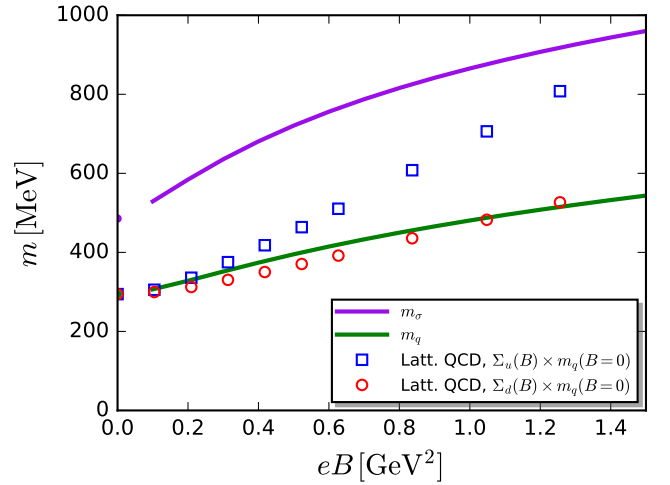


FIG. 5: Quark mass as a function of the strength of magnetic fields. The lattice QCD results are constructed from the quark chiral condensates in Ref [20]. The  $\sigma$  meson mass is also plotted.

with the magnetic field, while the sigma meson mass increases monotonically due to their internal structure. The decay constant and the light quark mass also increase with the magnetic field, reflecting the magnetic catalysis behavior at vanishing temperature. The neutral pion mass and pion decay constant are quantitatively in agreement with the lattice QCD results especially in the range of  $eB < 1.2 \text{ GeV}^2$ . However, the charged pion mass is in agreement with the lattice results in [17] but no non-monotonic mass behavior for charged pion

has been observed in this framework as shown in [20]. This needs further investigation from both lattice QCD and functional methods.

It is noteworthy that this is our first preliminary attempt to calculate meson masses and the pion decay constant in the QM model under strong magnetic fields within the FRG approach, and there are many things we need to do in the future. In the upcoming work, we will go beyond the LPA truncation, which includes the

magnetic dependent Yukawa couplings and wave function renormalizations, and calculate the spectral functions of the mesons. After that, we will extend them into finite temperatures and chemical potential. The strange quark and vector meson will also be included in future work.

### ACKNOWLEDGMENTS

We thank Chuang Huang, Jie Mei, Yang-yang Tan and Kun Xu for their valuable discussions. This work is supported in part by the National Natural Science Foundation of China (NSFC) Grant Nos: 12235016, 12221005, 12175030 and the Strategic Priority Research Program of Chinese Academy of Sciences under Grant No XDB34030000, the start-up funding from University of Chinese Academy of Sciences(UCAS), and the Fundamental Research Funds for the Central Universities.

### Appendix A: Vertexes

As mentioned above, we need the n-point vertexes to calculate the neutral and charged pion two-point correlation function [Equations \(17\) and \(18\)](#). The n-point vertexes are defined as

$$V_{\phi_1, \phi_2 \dots \phi_n} = \frac{\partial^n \Gamma_k}{\partial \phi_1 \partial \phi_2 \dots \partial \phi_n}. \quad (\text{A1})$$

The quark-meson interaction in the 2-flavor QM model reads

$$V_{\bar{u}d\pi^+} = V_{\bar{d}u\pi^-} = \frac{\sqrt{2}}{2} h i \gamma_5 \quad (\text{A2})$$

$$V_{\bar{u}u\pi^0} = V_{\bar{d}d\pi^0} = \frac{1}{2} h i \gamma_5 \quad (\text{A3})$$

$$V_{\bar{u}u\sigma} = V_{\bar{d}d\sigma} = \frac{1}{2} h. \quad (\text{A4})$$

The nonvanishing mesonic three-point and four-point vertexes are

$$V_{2\pi^\pm\sigma} = V_{2\pi^0\sigma} = \sigma V''(\rho) \quad (\text{A5})$$

$$V_{3\sigma} = 3\sigma V''(\rho) + \sigma^3 V'''(\rho) \quad (\text{A6})$$

$$V_{2\pi^\pm 2\sigma} = V_{2\pi^0 2\sigma} = V''(\rho) + \sigma^2 V'''(\rho) \quad (\text{A7})$$

$$V_{2\pi^\pm 2\pi^0} = V''(\rho) \quad (\text{A8})$$

$$V_{4\pi^0} = 3V''(\rho) \quad (\text{A9})$$

$$V_{4\pi^\pm} = 2V''(\rho). \quad (\text{A10})$$

### Appendix B: loop functions

The threshold functions of the effective potential for neutral meson  $\pi^0, \sigma$  in [Equation \(16\)](#) read

$$l_B(m_\phi) = \frac{k^4}{16\pi^2} (\log(k^2 + m_\phi^2 + \Lambda_\perp^2) - \log(k^2 + m_\phi^2)). \quad (\text{B1})$$

For the charged pion under magnetic fields, the threshold function is

$$l_B(m_\phi) = \frac{k^4}{8\pi^2} |q_\phi B| \sum_{n=0}^{\Lambda_\perp, n} \frac{1}{k^2 + m_\phi^2 + (2n+1)|q_\phi B|}. \quad (\text{B2})$$

The quark loop function for the effective potential in the vacuum:

$$l_F = \frac{k^4}{16\pi^2} \left( \log(k^2 + m_f^2 + \Lambda_\perp^2) - \log(k^2 + m_f^2) \right), \quad (\text{B3})$$

and the quark loop threshold function under magnetic fields reads

$$l_F = \frac{k^4}{16\pi^2} |q_f B| \sum_{n=0}^{\Lambda_\perp, n} \sum_{s=\pm 1} \frac{1}{k^2 + m_f^2 + |q_f B|(2n+1+s)}. \quad (\text{B4})$$

The loop function of the tadpole diagram in weak-field expansion reads

$$\begin{aligned} \mathcal{J}_B(\phi) = & \frac{k^4}{8\pi^2} \left[ -\frac{\Lambda_\perp^2}{(k^2 + m_\phi^2)(k^2 + m_\phi^2 + \Lambda_\perp^2)} \right. \\ & + \left( \frac{1}{3(k^2 + m_\phi^2)^3} - \frac{k^2 + m_\phi^2 - 5\Lambda_\perp^2}{3(k^2 + m_\phi^2 + \Lambda_\perp^2)^4} \right) (q_\phi B)^2 \\ & \left. + \mathcal{O}(q_\phi B)^4 \right]. \end{aligned} \quad (\text{B5})$$

For the loop functions of neutral meson, we just need to set  $q_\phi = 0$ . And loop functions of the charge pion in Landau level representation reads

$$\mathcal{J}_B(\phi) = -\frac{k^4 |q_\phi B|}{4\pi^2} \sum_{n=0}^{\Lambda_\perp, n} \frac{1}{k^2 + (2n+1)|q_\phi B| + m_\phi^2}. \quad (\text{B6})$$

The  $\sigma - \pi$  loop functions in weak-field expansion read

$$\begin{aligned} \mathcal{J}_{2B}(\pi, \sigma) = & \frac{k^4}{8\pi^2} \left[ \left( \frac{1}{(k^2 + m_\sigma^2 + \Lambda_\perp^2)(k^2 + m_\pi^2 + \Lambda_\perp^2)} \right. \right. \\ & - \frac{1}{(k^2 + m_\sigma^2)(k^2 + m_\pi^2)} \Big) \\ & - \int_0^{\Lambda_\perp^2} \left( \frac{5p_\perp^2 - 3m_\pi^2 - 3k^2}{(k^2 + m_\pi^2 + p_\perp^2)^5 (k^2 + m_\sigma^2 + p_\perp^2)} \right. \\ & \left. \left. + \frac{p_\perp^2 - k^2 - m_\pi^2}{(k^2 + m_\pi^2 + p_\perp^2)^4 (k^2 + m_\sigma^2 + p_\perp^2)^2} \right) dp_\perp^2 (q_\pi B)^2 \right. \\ & \left. + \mathcal{O}(q_\pi B)^4 \right] \end{aligned} \quad (\text{B7})$$

with neutral pion  $q_{\pi^0} = 0$  and charged pion  $q_{\pi^\pm} = \pm e$ .

The  $\sigma - \pi^\pm$  loop function in Landau level representation reads

$$\mathcal{J}_{2B}(\pi^\pm, \sigma) = -\frac{k^4}{4\pi^2} \sum_{n=0}^{\Lambda_{\perp,n}} \left( \frac{1}{(k^2 + (2n+1)|eB| + m_\pi^2)^2} \int_0^\infty \frac{e^{-y} \mathcal{L}_n(2y) dy}{y^2 + (k^2 + m_\sigma^2)/|eB|} + \frac{1}{(k^2 + (2n+1)|eB| + m_\pi^2)|eB|} \int_0^\infty \frac{e^{-y} \mathcal{L}_n(2y) dy}{(y^2 + (k^2 + m_\sigma^2)/|eB|)^2} \right) \quad (\text{B8})$$

The weak-field expansion of quark loop of the two-point correction of pion have shown in Equation (21) and Equation (22). If we set  $B = 0$ , they will come back to the representations of vacuum case.

In Landau level representation, the quark loop threshold functions of the neutral pion become

$$\mathcal{J}_{2F}(q_f) = \frac{k^4 N_c}{2\pi^2} \sum_{n=0}^{\Lambda_{\perp,n}} \sum_{s=\pm 1} \frac{1}{(k^2 + m_f^2 + |q_f B|(2n+1+s))^2} \quad (\text{B9})$$

For the charged pion two-point correction, it contains a  $u - d$  quark loop. The threshold function of this diagram

reads

$$\mathcal{J}_{2F}(u, d) = \frac{N_c k^4 B}{\pi^2} \sum_{n_1, n_2}^{\Lambda_{\perp,n}} (-1)^{(n_1+n_2)} [(\bar{G}_{n_1}^u)^2 \bar{G}_{n_2}^d + \bar{G}_{n_1}^u (\bar{G}_{n_2}^d)^2 ((k^2 + m_f^2)(LL(n_1, n_2 - 1) + LL(n_1 - 1, n_2)) - 8BL^1 L^1(n_1 - 1, n_2 - 1)) - \bar{G}_{n_1}^u \bar{G}_{n_2}^d (LL(n_1, n_2 - 1) + LL(n_1 - 1, n_2))] \quad (\text{B10})$$

here

$$\bar{G}_n^{q_f} \equiv \frac{1}{k^2 + m_f^2 + 2n|q_f B|} \quad (\text{B11})$$

where we also define the  $LL(n_1, n_2)$  and  $L^1 L^1(n_1, n_2)$  as the integrations of perpendicular direction

$$LL(n_1, n_2) \equiv \int_0^\infty dx \exp(-x(\frac{1}{|q_u|} + \frac{1}{|q_d|})) \quad (\text{B12})$$

$$\mathcal{L}_{n_1}(\frac{2x}{|q_u|}) \mathcal{L}_{n_2}(\frac{2x}{|q_d|})$$

$$L^1 L^1(n_1, n_2) \equiv \int_0^\infty dx x \exp(-x(\frac{1}{|q_u|} + \frac{1}{|q_d|})) \quad (\text{B13})$$

$$\mathcal{L}_{n_1}^1(\frac{2x}{|q_u|}) \mathcal{L}_{n_2}^1(\frac{2x}{|q_d|}),$$

with  $\mathcal{L}_n^a(x)$  are the generalized Laguerre polynomials.

- 
- [1] V. Skokov, A. Y. Illarionov, and V. Toneev, Estimate of the magnetic field strength in heavy-ion collisions, *Int. J. Mod. Phys. A* **24**, 5925 (2009), arXiv:0907.1396 [nucl-th].
- [2] W.-T. Deng and X.-G. Huang, Event-by-event generation of electromagnetic fields in heavy-ion collisions, *Phys. Rev. C* **85**, 044907 (2012), arXiv:1201.5108 [nucl-th].
- [3] T. Vachaspati, Magnetic fields from cosmological phase transitions, *Phys. Lett. B* **265**, 258 (1991).
- [4] R. Durrer and A. Neronov, Cosmological Magnetic Fields: Their Generation, Evolution and Observation, *Astron. Astrophys. Rev.* **21**, 62 (2013), arXiv:1303.7121 [astro-ph.CO].
- [5] K. Kiuchi, P. Cerdá-Durán, K. Kyutoku, Y. Sekiguchi, and M. Shibata, Efficient magnetic-field amplification due to the Kelvin-Helmholtz instability in binary neutron star mergers, *Phys. Rev. D* **92**, 124034 (2015), arXiv:1509.09205 [astro-ph.HE].
- [6] D. E. Kharzeev, L. D. McLerran, and H. J. Warringa, The Effects of topological charge change in heavy ion collisions: 'Event by event P and CP violation', *Nucl. Phys. A* **803**, 227 (2008), arXiv:0711.0950 [hep-ph].
- [7] D. E. Kharzeev and D. T. Son, Testing the chiral magnetic and chiral vortical effects in heavy ion collisions, *Phys. Rev. Lett.* **106**, 062301 (2011), arXiv:1010.0038 [hep-ph].
- [8] S. P. Klevansky and R. H. Lemmer, Chiral symmetry restoration in the Nambu-Jona-Lasinio model with a constant electromagnetic field, *Phys. Rev. D* **39**, 3478 (1989).
- [9] K. G. Klimenko, Three-dimensional Gross-Neveu model in an external magnetic field, *Teor. Mat. Fiz.* **89**, 211 (1991).
- [10] V. P. Gusynin, V. A. Miransky, and I. A. Shovkovy, Dimensional reduction and catalysis of dynamical symmetry breaking by a magnetic field, *Nucl. Phys. B* **462**, 249 (1996), arXiv:hep-ph/9509320.
- [11] G. S. Bali, F. Bruckmann, G. Endrodi, Z. Fodor, S. D. Katz, and A. Schafer, QCD quark condensate in external magnetic fields, *Phys. Rev. D* **86**, 071502 (2012), arXiv:1206.4205 [hep-lat].
- [12] A. Tomiya, H.-T. Ding, X.-D. Wang, Y. Zhang, S. Mukherjee, and C. Schmidt, Phase structure of three flavor QCD in external magnetic fields using HISQ fermions, *PoS LATTICE2018*, 163 (2019), arXiv:1904.01276 [hep-lat].
- [13] J. O. Andersen, QCD phase diagram in a constant magnetic background: Inverse magnetic catalysis: where models meet the lattice, *Eur. Phys. J. A* **57**, 189 (2021), arXiv:2102.13165 [hep-ph].
- [14] G. S. Bali, F. Bruckmann, G. Endrödi, S. D. Katz, and A. Schäfer, The QCD equation of state in background magnetic fields, *JHEP* **08**, 177, arXiv:1406.0269 [hep-lat].
- [15] G. S. Bali, F. Bruckmann, M. Constantinou, M. Costa, G. Endrodi, S. D. Katz, H. Panagopoulos, and A. Schafer, Magnetic susceptibility of QCD at zero and at finite

- temperature from the lattice, *Phys. Rev. D* **86**, 094512 (2012), [arXiv:1209.6015 \[hep-lat\]](#).
- [16] G. S. Bali, F. Bruckmann, G. Endrodi, Z. Fodor, S. D. Katz, S. Krieg, A. Schafer, and K. K. Szabo, The QCD phase diagram for external magnetic fields, *JHEP* **02**, 044, [arXiv:1111.4956 \[hep-lat\]](#).
- [17] G. S. Bali, B. B. Brandt, G. Endrődi, and B. Gläsel, Meson masses in electromagnetic fields with Wilson fermions, *Phys. Rev. D* **97**, 034505 (2018), [arXiv:1707.05600 \[hep-lat\]](#).
- [18] R. Bignell, W. Kamleh, and D. Leinweber, Pion magnetic polarisability using the background field method, *Phys. Lett. B* **811**, 135853 (2020), [arXiv:2005.10453 \[hep-lat\]](#).
- [19] V. G. Bornyakov, P. V. Buividovich, N. Cundy, O. A. Kochetkov, and A. Schäfer, Deconfinement transition in two-flavor lattice QCD with dynamical overlap fermions in an external magnetic field, *Phys. Rev. D* **90**, 034501 (2014), [arXiv:1312.5628 \[hep-lat\]](#).
- [20] H. T. Ding, S. T. Li, A. Tomiya, X. D. Wang, and Y. Zhang, Chiral properties of (2+1)-flavor QCD in strong magnetic fields at zero temperature, *Phys. Rev. D* **104**, 014505 (2021), [arXiv:2008.00493 \[hep-lat\]](#).
- [21] H. T. Ding, S. T. Li, J. H. Liu, and X. D. Wang, Chiral condensates and screening masses of neutral pseudoscalar mesons in thermomagnetic QCD medium, *Phys. Rev. D* **105**, 034514 (2022), [arXiv:2201.02349 \[hep-lat\]](#).
- [22] T. Inagaki, D. Kimura, and T. Murata, Four fermion interaction model in a constant magnetic field at finite temperature and chemical potential, *Prog. Theor. Phys.* **111**, 371 (2004), [arXiv:hep-ph/0312005](#).
- [23] J. Chao, L. Yu, and M. Huang, Zeta function regularization of the photon polarization tensor for a magnetized vacuum, *Phys. Rev. D* **90**, 045033 (2014), [Erratum: *Phys. Rev. D* **91**, 029903 (2015)], [arXiv:1403.0442 \[hep-th\]](#).
- [24] L. Yu, J. Van Doorselaere, and M. Huang, Inverse Magnetic Catalysis in the three-flavor NJL model with axial-vector interaction, *Phys. Rev. D* **91**, 074011 (2015), [arXiv:1411.7552 \[hep-ph\]](#).
- [25] M. Coppola, D. Gómez Dumm, and N. N. Scoccola, Charged pion masses under strong magnetic fields in the NJL model, *Phys. Lett. B* **782**, 155 (2018), [arXiv:1802.08041 \[hep-ph\]](#).
- [26] M. Coppola, D. Gomez Dumm, S. Noguera, and N. N. Scoccola, Neutral and charged pion properties under strong magnetic fields in the NJL model, *Phys. Rev. D* **100**, 054014 (2019), [arXiv:1907.05840 \[hep-ph\]](#).
- [27] S. Fayazbakhsh and N. Sadooghi, Anomalous magnetic moment of hot quarks, inverse magnetic catalysis, and reentrance of the chiral symmetry broken phase, *Phys. Rev. D* **90**, 105030 (2014), [arXiv:1408.5457 \[hep-ph\]](#).
- [28] N. Chaudhuri, S. Ghosh, S. Sarkar, and P. Roy, Effect of the anomalous magnetic moment of quarks on the phase structure and mesonic properties in the NJL model, *Phys. Rev. D* **99**, 116025 (2019), [arXiv:1907.03990 \[nucl-th\]](#).
- [29] A. Ayala, R. L. S. Farias, S. Hernández-Ortiz, L. A. Hernández, D. M. Paret, and R. Zamora, Magnetic field-dependence of the neutral pion mass in the linear sigma model coupled to quarks: The weak field case, *Phys. Rev. D* **98**, 114008 (2018), [arXiv:1809.08312 \[hep-ph\]](#).
- [30] K. Kamikado and T. Kanazawa, Chiral dynamics in a magnetic field from the functional renormalization group, *JHEP* **03**, 009, [arXiv:1312.3124 \[hep-ph\]](#).
- [31] K. Kamikado and T. Kanazawa, Magnetic susceptibility of a strongly interacting thermal medium with 2+1 quark flavors, *JHEP* **01**, 129, [arXiv:1410.6253 \[hep-ph\]](#).
- [32] K. A. Mamo, Inverse magnetic catalysis in holographic models of QCD, *JHEP* **05**, 121, [arXiv:1501.03262 \[hep-th\]](#).
- [33] D. Li, M. Huang, Y. Yang, and P.-H. Yuan, Inverse Magnetic Catalysis in the Soft-Wall Model of AdS/QCD, *JHEP* **02**, 030, [arXiv:1610.04618 \[hep-th\]](#).
- [34] K. Fukushima and J. M. Pawłowski, Magnetic catalysis in hot and dense quark matter and quantum fluctuations, *Phys. Rev. D* **86**, 076013 (2012), [arXiv:1203.4330 \[hep-ph\]](#).
- [35] J. Braun, W. A. Mian, and S. Rechenberger, Delayed Magnetic Catalysis, *Phys. Lett. B* **755**, 265 (2016), [arXiv:1412.6025 \[hep-ph\]](#).
- [36] N. Mueller and J. M. Pawłowski, Magnetic catalysis and inverse magnetic catalysis in QCD, *Phys. Rev. D* **91**, 116010 (2015), [arXiv:1502.08011 \[hep-ph\]](#).
- [37] W.-j. Fu and Y.-x. Liu, Four-fermion interactions and the chiral symmetry breaking in an external magnetic field, *Phys. Rev. D* **96**, 074019 (2017), [arXiv:1705.09841 \[hep-ph\]](#).
- [38] X. Li, W.-J. Fu, and Y.-X. Liu, Thermodynamics of 2+1 Flavor Polyakov-Loop Quark-Meson Model under External Magnetic Field, *Phys. Rev. D* **99**, 074029 (2019), [arXiv:1902.03866 \[hep-ph\]](#).
- [39] I. A. Shovkovy, Magnetic Catalysis: A Review, *Lect. Notes Phys.* **871**, 13 (2013), [arXiv:1207.5081 \[hep-ph\]](#).
- [40] J. O. Andersen, W. R. Naylor, and A. Tranberg, Phase diagram of QCD in a magnetic field: A review, *Rev. Mod. Phys.* **88**, 025001 (2016), [arXiv:1411.7176 \[hep-ph\]](#).
- [41] V. A. Miransky and I. A. Shovkovy, Quantum field theory in a magnetic field: From quantum chromodynamics to graphene and Dirac semimetals, *Phys. Rept.* **576**, 1 (2015), [arXiv:1503.00732 \[hep-ph\]](#).
- [42] K. Hattori, K. Itakura, and S. Ozaki, Strong-Field Physics in QED and QCD: From Fundamentals to Applications, (2023), [arXiv:2305.03865 \[hep-ph\]](#).
- [43] K. Fukushima and Y. Hidaka, Magnetic Catalysis Versus Magnetic Inhibition, *Phys. Rev. Lett.* **110**, 031601 (2013), [arXiv:1209.1319 \[hep-ph\]](#).
- [44] S. Mao, Inverse magnetic catalysis in Nambu–Jona-Lasinio model beyond mean field, *Phys. Lett. B* **758**, 195 (2016), [arXiv:1602.06503 \[hep-ph\]](#).
- [45] E. V. Luschevskaya, O. E. Solovjeva, and O. V. Teryaev, Determination of the properties of vector mesons in external magnetic field by Quenched  $SU(3)$  Lattice QCD, *JHEP* **09**, 142, [arXiv:1608.03472 \[hep-lat\]](#).
- [46] Z. Wang and P. Zhuang, Meson properties in magnetized quark matter, *Phys. Rev. D* **97**, 034026 (2018), [arXiv:1712.00554 \[hep-ph\]](#).
- [47] H. Liu, X. Wang, L. Yu, and M. Huang, Neutral and charged scalar mesons, pseudoscalar mesons, and diquarks in magnetic fields, *Phys. Rev. D* **97**, 076008 (2018), [arXiv:1801.02174 \[hep-ph\]](#).
- [48] A. Ayala, J. L. Hernández, L. A. Hernández, R. L. S. Farias, and R. Zamora, Magnetic field dependence of the neutral pion mass in the linear sigma model with quarks: The strong field case, *Phys. Rev. D* **103**, 054038 (2021), [arXiv:2011.03673 \[hep-ph\]](#).
- [49] Y. Hidaka and A. Yamamoto, Charged vector mesons in a strong magnetic field, *Phys. Rev. D* **87**, 094502 (2013), [arXiv:1209.0007 \[hep-ph\]](#).
- [50] J. Li, G. Cao, and L. He, Gauge independence of pion masses in a magnetic field within the Nambu–Jona-

- Lasinio model, *Phys. Rev. D* **104**, 074026 (2021), [arXiv:2009.04697 \[nucl-th\]](#).
- [51] J. P. Carlomagno, D. Gomez Dumm, M. F. I. Villafañe, S. Noguera, and N. N. Scoccola, Charged pseudoscalar and vector meson masses in strong magnetic fields in an extended NJL model, *Phys. Rev. D* **106**, 094035 (2022), [arXiv:2209.10679 \[hep-ph\]](#).
- [52] G. Endrődi and G. Markó, Magnetized baryons and the QCD phase diagram: NJL model meets the lattice, *JHEP* **08**, 036, [arXiv:1905.02103 \[hep-lat\]](#).
- [53] K. Xu, J. Chao, and M. Huang, Effect of the anomalous magnetic moment of quarks on magnetized QCD matter and meson spectra, *Phys. Rev. D* **103**, 076015 (2021), [arXiv:2007.13122 \[hep-ph\]](#).
- [54] F. Lin, K. Xu, and M. Huang, Magnetism of QCD matter and the pion mass from tensor-type spin polarization and the anomalous magnetic moment of quarks, *Phys. Rev. D* **106**, 016005 (2022), [arXiv:2202.03226 \[hep-ph\]](#).
- [55] Z. Xing, J. Chao, L. Chang, and Y.-x. Liu, Exposing the effect of the p-wave component in the pion triplet under a strong magnetic field, *Phys. Rev. D* **105**, 114003 (2022), [arXiv:2110.01245 \[hep-ph\]](#).
- [56] T. Kojo, Neutral and charged mesons in magnetic fields: A resonance gas in a non-relativistic quark model, *Eur. Phys. J. A* **57**, 317 (2021), [arXiv:2104.00376 \[hep-ph\]](#).
- [57] B. Sheng, Y. Wang, X. Wang, and L. Yu, Pole and screening masses of neutral pions in a hot and magnetized medium: A comprehensive study in the Nambu–Jona-Lasinio model, *Phys. Rev. D* **103**, 094001 (2021), [arXiv:2010.05716 \[hep-ph\]](#).
- [58] J. Mei, T. Xia, and S. Mao, Mass spectra of neutral mesons  $K_0$ ,  $\pi_0$ ,  $\eta$ ,  $\eta'$  at finite magnetic field, temperature and baryon chemical potential, (2022), [arXiv:2212.04778 \[hep-ph\]](#).
- [59] J. Mei and S. Mao, Inverse catalysis effect of the quark anomalous magnetic moment to chiral restoration and deconfinement phase transitions, *Phys. Rev. D* **102**, 114035 (2020), [arXiv:2008.12123 \[hep-ph\]](#).
- [60] C. A. Islam, M. S. Ali, and M. Huang, Deciding on the anomalous magnetic moment of quarks in a framework of nonlocal NJL model, (2023), [arXiv:2302.00696 \[hep-ph\]](#).
- [61] A. Das and N. Haque, Neutral pion mass in the linear sigma model coupled to quarks at arbitrary magnetic field, *Phys. Rev. D* **101**, 074033 (2020), [arXiv:1908.10323 \[hep-ph\]](#).
- [62] B.-J. Schaefer and J. Wambach, The Phase diagram of the quark meson model, *Nucl. Phys. A* **757**, 479 (2005), [arXiv:nucl-th/0403039](#).
- [63] Y.-r. Chen, R. Wen, and W.-j. Fu, Critical behaviors of the O(4) and Z(2) symmetries in the QCD phase diagram, *Phys. Rev. D* **104**, 054009 (2021), [arXiv:2101.08484 \[hep-ph\]](#).
- [64] B.-J. Schaefer and H.-J. Pirner, Renormalization group flow and equation of state of quarks and mesons, *Nucl. Phys. A* **660**, 439 (1999), [arXiv:nucl-th/9903003](#).
- [65] T. K. Herbst, M. Mitter, J. M. Pawłowski, B.-J. Schaefer, and R. Stiele, Thermodynamics of QCD at vanishing density, *Phys. Lett. B* **731**, 248 (2014), [arXiv:1308.3621 \[hep-ph\]](#).
- [66] R. Wen, C. Huang, and W.-J. Fu, Baryon number fluctuations in the 2+1 flavor low energy effective model, *Phys. Rev. D* **99**, 094019 (2019), [arXiv:1809.04233 \[hep-ph\]](#).
- [67] W.-j. Fu, X. Luo, J. M. Pawłowski, F. Rennecke, R. Wen, and S. Yin, Hyper-order baryon number fluctuations at finite temperature and density, (2021), [arXiv:2101.06035 \[hep-ph\]](#).
- [68] J. Hubbard, Calculation of partition functions, *Phys. Rev. Lett.* **3**, 77 (1959).
- [69] C. Jung, F. Rennecke, R.-A. Tripolt, L. von Smekal, and J. Wambach, In-Medium Spectral Functions of Vector- and Axial-Vector Mesons from the Functional Renormalization Group, *Phys. Rev. D* **95**, 036020 (2017), [arXiv:1610.08754 \[hep-ph\]](#).
- [70] N. Dupuis, L. Canet, A. Eichhorn, W. Metzner, J. M. Pawłowski, M. Tissier, and N. Wschebor, The nonperturbative functional renormalization group and its applications, *Phys. Rept.* **910**, 1 (2021), [arXiv:2006.04853 \[cond-mat.stat-mech\]](#).
- [71] J. M. Pawłowski, Aspects of the functional renormalisation group, *Annals Phys.* **322**, 2831 (2007), [arXiv:hep-th/0512261](#).
- [72] W.-j. Fu, J. M. Pawłowski, and F. Rennecke, QCD phase structure at finite temperature and density, *Phys. Rev. D* **101**, 054032 (2020), [arXiv:1909.02991 \[hep-ph\]](#).
- [73] J. Braun, L. Fister, J. M. Pawłowski, and F. Rennecke, From Quarks and Gluons to Hadrons: Chiral Symmetry Breaking in Dynamical QCD, *Phys. Rev. D* **94**, 034016 (2016), [arXiv:1412.1045 \[hep-ph\]](#).
- [74] A. J. Helmboldt, J. M. Pawłowski, and N. Strodthoff, Towards quantitative precision in the chiral crossover: masses and fluctuation scales, *Phys. Rev. D* **91**, 054010 (2015), [arXiv:1409.8414 \[hep-ph\]](#).
- [75] J. O. Andersen, W. R. Naylor, and A. Tranberg, Chiral and deconfinement transitions in a magnetic background using the functional renormalization group with the Polyakov loop, *JHEP* **04**, 187, [arXiv:1311.2093 \[hep-ph\]](#).
- [76] C. Wetterich, Exact evolution equation for the effective potential, *Phys. Lett. B* **301**, 90 (1993), [arXiv:1710.05815 \[hep-th\]](#).
- [77] S. Yin, R. Wen, and W.-j. Fu, Mesonic dynamics and the QCD phase transition, *Phys. Rev. D* **100**, 094029 (2019), [arXiv:1907.10262 \[hep-ph\]](#).
- [78] G. Cao, Recent progresses on QCD phases in a strong magnetic field: views from Nambu–Jona-Lasinio model, *Eur. Phys. J. A* **57**, 264 (2021), [arXiv:2103.00456 \[hep-ph\]](#).
- [79] J. S. Schwinger, On gauge invariance and vacuum polarization, *Phys. Rev.* **82**, 664 (1951).
- [80] S. Mao, Pions in magnetic field at finite temperature, *Phys. Rev. D* **99**, 056005 (2019), [arXiv:1808.10242 \[nucl-th\]](#).
- [81] T.-K. Chyi, C.-W. Hwang, W. F. Kao, G.-L. Lin, K.-W. Ng, and J.-J. Tseng, The weak field expansion for processes in a homogeneous background magnetic field, *Phys. Rev. D* **62**, 105014 (2000), [arXiv:hep-th/9912134](#).
- [82] A. Ayala, M. Loewe, and R. Zamora, Inverse magnetic catalysis in the linear sigma model with quarks, *Phys. Rev. D* **91**, 016002 (2015), [arXiv:1406.7408 \[hep-ph\]](#).
- [83] A. Ayala, A. Sanchez, G. Piccinelli, and S. Sahu, Effective potential at finite temperature in a constant magnetic field. I. Ring diagrams in a scalar theory, *Phys. Rev. D* **71**, 023004 (2005), [arXiv:hep-ph/0412135](#).
- [84] J. M. Pawłowski and F. Rennecke, Higher order quark-mesonic scattering processes and the phase structure of QCD, *Phys. Rev. D* **90**, 076002 (2014), [arXiv:1403.1179 \[hep-ph\]](#).